Electron-impact single and double ionization of Ba^{2+} and Ba^{3+} ions

K. Tinschert,* A. Müller, G. Hofmann, and E. Salzborn
Institut für Kernphysik, Universität Giessen, D-6300 Giessen, Federal Republic of Germany

S. M. Younger
Los Alamos National Laboratory, Los Alamos, New Mexico 87545
(Received 24 August 1990)

Experimental cross sections for single and double ionization of Ba^{2+} and Ba^{3+} ions are presented for an electron-impact energy range from threshold up to 1000 eV. By the alternative use of a "hot" electron-cyclotron-resonance ion source and a "cold" Penning ion source, beams of ions with and without metastable content could be employed. A fast energy-scanning technique with step widths of about 40 meV and an energy resolution of 0.4 eV revealed fine details in the cross sections, and in particular resonant contributions to single and double ionization could be observed. The data are interpreted on the basis of calculations of energy levels and distorted-wave calculations of direct ionization from various electron subshells. Influences of giant-resonance phenomena are discussed.

I. INTRODUCTION

Barium and its close neighbors in the Periodic Table of elements have an electronic structure that provides unique phenomena in photoabsorption and electron-impact ionization. In particular, large resonance structures caused by $4d \rightarrow \epsilon f$ excitations have attracted great interest in studies of photoionization of Ba and the lanthanide elements. The characteristics of these elements are determined by the role of the $4f$ subshell. Subsequent to the classical work of Goeppert-Mayer,[1] who used Thomas-Fermi potentials to predict the onset of the rare-earth series, effective central potentials for $4f$ electrons were calculated by inverting Hartree-Fock calculations.[2] These effective potentials have pronounced double-well structures for the outer d and f electrons. For neutral atoms with atomic numbers $Z < 57$ the potential barrier separating the two wells keeps the $4f$ wave function outside the region occupied by the core electrons. At $Z = 57$ the barrier becomes low enough so that the $4f$ orbital suddenly contracts (wave-function collapse) and resides in the inner well of the effective potential.[2] The question of whether an orbital is collapsed or not often depends on the particular term in a given configuration which leads to strong differences in oscillator strengths of different terms.[3] Extreme term dependence has been shown in $4d^9 4f$ configurations within the palladium sequence.[4]

In 1964 Ederer[5] published his work on the photoionization of Xe, where he found an unexpected photon-energy dependence in the $4d$ cross section. A pronounced peak in the cross section at around 100 eVwas observed. Similar features were also found[6] in the photoionization of Ba and other atoms and ions. These peak structures are generally termed "giant resonances." Since the first observations numerous experiments on the photoionization of Ba and its ions as well as related theoretical studies have been published. Recent papers were presented by Bizau *et al.*[7] and Richter *et al.*[8] The field has been previously reviewed in a book edited by Connerade, Esteva, and Karnatac.[9]

Over the past few years, the electron-impact ionization of very heavy ions has been the focus of several crossed beam measurements. In some of these experiments[10–14] large anomalous features at electron energies less than two times the threshold energy were found for double ionization of ions with atomic numbers close to $Z = 56$ (Ba). Pindzola *et al.*[15,16] could reproduce such features along the Xe^{q+} isonuclear sequence by performing distorted-wave calculations including term-dependent and correlation effects. Younger[17] interpreted a similar feature in Cs^+ as a giant scattering resonance appearing in the scattered-electron channel. Systematic theoretical studies of giant resonance phenomena for a variety of heavy ions in low charge states followed.[18–20] Recently, Müller *et al.*[21] presented a comprehensive study of single and multiple ionization of La^{q+} ions ($q = 1,2,3$). In that work giant-resonance phenomena were discussed along with other aspects of electron-impact ionization of heavy-metal ions. Experimentally, narrow resonances were also found clearly indicating the presence of resonant-excitation double autoionization[22] (REDA), i.e., dielectronic capture of the projectile electron and subsequent sequential emission of two electrons. It was even possible to identify resonant contributions to net double ionization,[14,21] i.e., resonant-excitation triple autoionization (RETA). Previous experimental and theoretical studies on electron-impact ionization of Ba^+ ions can be found in Refs. 13 and 23–27.

The present investigation continues a series of papers reporting on detailed studies of electron-impact ionization of heavy-metal ions. Some of the present results were already published in a Letter[14] where space was not sufficient to discuss details of the experiment. We report here complete cross-section measurements from threshold up to 1000 eV for single and double ionization of

Ba^{2+} and Ba^{3+} ions, as well as additional high-resolution energy scans. By using different ions sources, beams with different metastable ion contents could be employed in the measurements and additional information on the ionization of metastable excited states was obtained. Distorted-wave calculations for direct single ionization of different electron subshells in Ba^{2+} and Ba^{3+} were performed with comprehensive calculations of energy levels of ions along the Ba^{q+} isonuclear sequence.

II. EXPERIMENTAL METHODS

The experimental data were taken by using the Giessen electron-ion crossed-beam apparatus. The present setup was recently described in detail.[28]

The Ba^{2+} and Ba^{3+} ions were produced by two types of ion sources, a "cold" sputter Penning ion source[29] (PIG) and a "hot" electron-cyclotron-resonance (ECR) ion source.[30] Here "cold" and "hot" refer qualitatively to the electron energies in these sources and their capability to produce highly excited ionic species. The Penning source worked with an Ar discharge typically running with 50 mA at several hundred volts. The anticathode contained an inlay of metallic barium which was sputtered by Ar ions. Ba ions were extracted through a 1.5-mm channel in the cathode.

The two-stage ECR ion source was operated with a microwave frequency of 5 GHz. Metallic barium was evaporated in a direct-current heated molybdenum crucible. Through a slit of about 1×15 mm^2 Ba atoms effused into the plasma in the second stage of the ECR ion source.

Both sources were operated with an acceleration voltage of 10 kV so that the Ba^{2+} ions acquired 20 keV and the Ba^{3+} ions 30 keV of energy. After magnetic analysis, tight collimation to about 0.5 mm diam and transport to the collision region, several nA of beam current were obtained, which, due to the huge ionization cross sections, often had to be reduced further to the pA range.

The ion beam was crossed at right angle with an intense electron beam.[31] Ionized product ions were separated from the parent-ion beam by magnetic analysis and detected with a single-particle counter.[32] The parent-ion beam was collected in a wide Faraday cup inside the analyzing-magnet chamber.[33]

The electron gun provides a ribbon-shaped electron beam that extends 60 mm in the ion-beam direction. The gun is operated in space-charge limited mode and provides a current of about 15 mA at 100 eV and 460 mA at 1000 eV. The space-charge potential depression of such beams is quite substantial. For a 100-eV beam of 15-mA current a depression of 4 V would be expected between the edge and the center of the beam. This space-charge depression, however, is offset by filling the space-charge well with slow ions from Kr gas fed into the collision chamber. This gives an electron energy spread of 0.4 eV or better as evidenced by our experiments.[14] Even at electron currents as high as 300 mA (at 750 eV) the experimental energy spread was found to be less than 3 eV. The reproducibility of our energy measurements is within 0.5 eV. Comparisons with Auger-spectroscopy data suggest that our energy calibration is within deviations of not more than about 1 eV, even at 750 eV.[34]

For the measurement of cross sections we have employed two modes of data taking.

Mode 1. Absolute ionization cross sections were obtained by employing a technique wherein the electron gun is moved up and down across the ion beam, while the count rate of ionized ions, the ion current, the electron current, and the speed of the movement are recorded simultaneously in four different multi-channel analyzer (MCA) spectra with 512 channels each.[35] When the two beams cross each other the observed count rate is increased by the true ionization signal, leading to a peak in the spectrum. In the extreme positions of the electron gun the beams do not overlap and hence the observed count rate gives the experimental background that is due to stripping collisions in the residual gas and stray electrons or photons. After channel-by-channel division of the count rate by accumulated ion charge, the area S of the signal peak in the spectrum is determined and the cross section is calculated from

$$\sigma=\frac{S\Delta z}{MI_e\epsilon}K \ . \tag{1}$$

The constant K contains the conversion factors of beam currents to proportional frequencies and number of counts to accumulated ion charge; I_e is the electron current, and ϵ is the detection efficiency of the single-particle detector for the product ions. Each channel of the MCA spectra corresponds to a position interval $\Delta z=0.036$ mm. The dwell time for the one-half period of the electron-gun movement per interval Δz is about 0.1 s. The factor M is given by

$$M=(v_e^2+v_i^2)^{1/2}/v_e v_i q e^2 \ . \tag{2}$$

Here, v_e is the electron velocity, v_i is the ion velocity, q is the target ion charge state, and e is the charge of an electron. Details of this experimental technique have been described earlier.[35]

Mode 2. We have extended our data-taking program by adding a mode providing for fast energy scans with the electron gun in a fixed position, i.e., with fixed optimum overlap of the electron and ion beams. A digital-to-analog converter (DAC) was programmed to output a step function with 256 individual voltages. This step function was used with variable offset and amplification to control the energy of the electrons in the interaction region. Changing the energy and providing the necessary gate signals from the computer took about 10 ms. As a compromise between scan speed and efficient data collection, we chose a dwell time of about 50 ms on each electron energy. One scan spanned typically over 10 eV and took 17.5 s. Energy intervals were 0.039 eV. By repeating scans hundreds or even thousands of times, we averaged out possible fluctuations in the form factor, measurements of beam currents and counting rates, and fluctuations in others sources of data scatter. With the high cross sections for electron-impact ionization of the heavy ions studied and the intensity in our electron beam, it was usually possible to run with several thousand true signal

counts per second and nearly no background. Hence, statistical uncertainties on each energy point of less than 0.5% could be obtained within a few hours.

The combination of a high-intensity electron beam and a fast scanning technique that averages out systematic fluctuations in cross-section measurements allows us to sensibly accumulate signal counts and reduce the statistical uncertainty as well as systematic point-to-point data scatter. We have accumulated about 10^8 counts per channel in another experiment[36] and were able to reduce the point-to-point relative uncertainty to the 0.01% level. The remarkably low experimental energy spread in our cross-beam arrangement with a high-intensity electron gun thus provides an ideal prerequisite to observe fine details in ionization cross sections and thus to perform a new spectroscopy of intermediate excited states contributing to ionization processes involving single or multiple autoionization.

Though the point-to-point uncertainty in the relative scan measurements (mode 2) can be extremely low, the absolute uncertainty is limited by the absolute cross-section measurements (mode 1). In the scanning mode we do not have direct information about the form factor which determines the beam overlap. Also, the background is measured in separate runs with no overlap of the electron and ion beams. Time spans between the measurement of signal plus background and only background may be hours, so that an exact background subtraction cannot be guaranteed. A false subtraction of background, however, does not introduce spurious structure, since the background spectra (versus electron energy) are completely flat or at most slightly increasing with the electron current. Resulting uncertainties in the scan cross sections are substantially eliminated by normalizing them to the absolute measurements (mode 1). For the present experiments, normalization means the multiplication of all scan data by a constant factor to match the data with the absolute cross-section points. After all of these procedures, the absolute uncertainties of the scan data are close to those of the "normal" measurements (mode 1), i.e., 8–10%, while statistical uncertainties are typically lower than 0.5%.

Each absolute cross section taken by employing the mode-1 technique is typically determined from a single accumulated measurement. The quadrature sum of non-statistical uncertainties is 7.8% resulting from uncertainties in the detection efficiency (0.97 ± 0.03), the channel width Δz ($\pm1\%$), the ion and electron currents ($\pm5\%$

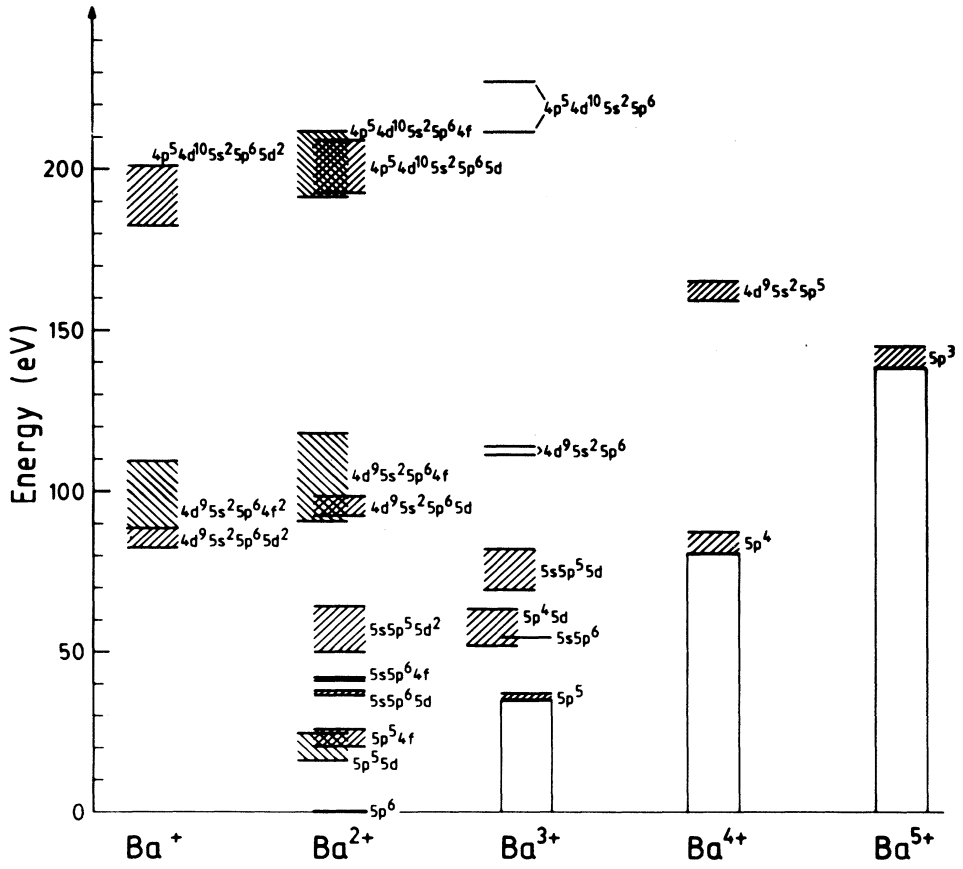

FIG. 1. Energy-level diagrams for Ba^{q+} ions ($q=1,2,\ldots,5$) relevant to the ionization of Ba ions. The configuration average energies were obtained by using the code of Grant, McKenzie, and Norrington (Ref. 45).

each), and the kinematic factor $M(\pm 1\%)$. Uncertainties in the ion and electron velocities are less than 1%. The total uncertainties are the quadrature sums of statistical and nonstatistical uncertainties. They amount to typically 8–10 % in these experiments.

III. THEORETICAL METHODS

The total single ionization cross section for an ion A^{q+} in the initial electronic state i, ignoring interference effects between the competing processes of direct ionization, excitation-autoionization, and resonant-recombination multiple-autoionization processes, may be written as

$$\sigma^{(\mathrm{tot})}_{q,q+1}(i)=\sum_f \sigma^{(\mathrm{ion})}_{q,q+1}(i\rightarrow f)B^r_f+\sum_j \sigma^{(\mathrm{exc})}_{q,q}(i\rightarrow j)B^a_j + \sum_k \sigma^{(\mathrm{cap})}_{q,q-1}(i\rightarrow k) \times \left[B^{2a}_k+\sum_m B^a_k(k\rightarrow m)B^a_m\right], \quad (3)$$

where j, k, and m denote autoionizing states.

Here $\sigma^{(\mathrm{ion})}_{q,q+1}(i\rightarrow f)$ is the direct-ionization cross section from the initial state i to a particular level f within the singly ionized configurations. In case f is an autoionizing state populated by inner-shell ionizations a branching ratio B^r_f has to be considered which describes the radiative stabilization of f leading to net single ionization with no further autoionization. The second term contains contributions $\sigma^{(\mathrm{exc})}_{q,q}(i\rightarrow j)$ for nonresonant excitation, i.e., excitation without change of the ion charge state, from the initial configuration to a particular autoionizing level j within the core-excited configurations. The quantity B^a_j is the branching ratio for (a single) autoionization from level j. The third term involves contributions from resonant excitation (dielectronic capture) from the initial state to a particular autoionizing level k within the core-excited configurations of the one less-charged ion. Such states decay by sequential (single) Auger (or Coster-Kronig) processes via different intermediate autoionizing states m. In addition, simultaneous emission of two electrons from state k has to be considered by a branch ratio B^{2a}_k.

Equation (3) shows that calculation of the cross sections $\sigma_{q,q+1}(i)=\sigma^{(\mathrm{tot})}_{q,q+1}(i)$ requires a substantial amount of information on atomic structure, the lifetimes and branching ratios of states, and collision dynamics. Few attempts have been made so far to assess all aspects of Eq. (3) for the ionization of heavy ions. The first example of such a calculation is that by LaGattuta and Hahn[37] on the ionization of Fe^{15+}. Later, Henry and Msezane[38] did close-coupling calculations for other sodiumlike ions, assuming unit branching ratios for autoionization. Calculations were done[39–42] more recently for other species and Fe^{15+} again.[43,44]

To guide the interpretation of the present experimental results for Ba ions, autoionizing energy-level and a limited number of direct-ionization calculations were carried out. Clearly, extensive theoretical work remains in order to properly interpret the complicated resonance structures observed.

For the computation of wave function and energy posi-

TABLE I. Total energies of levels relevant to ionization of Ba ions calculated by using the code of Grant, McKenzie, and Norrington (Ref. 45). For each configuration the number of levels is given with the range of total binding energies as well as the threshold energies for reaching these states from the $5p^6$ ground configuration and the $5p^5 5d$ excited configuration.

Charge state	Configuration	Number of levels	Energy (E) (eV)	$E-E(5p^6)$ (eV)	$E-E(5p^5 5d)$ (eV)
Ba^{2+}	$5p^6$	1	221 083.3	0	
Ba^{2+}	$5p^5 5d$	12	221 067.1–221 058.8	16.2–24.5	0
Ba^{2+}	$5p^5 4f$	12	221 061.8–221 057.5	21.5–25.8	
Ba^{3+}	$5p^5$	2	221 048.4–221 046.2	34.9–37.1	
Ba^{2+}	$5s5p^6 5d$	4	221 046.8–221 045.3	36.5–38.0	
Ba^{2+}	$5s5p^6 4f$	4	221 042.4–221 041.2	40.9–42.1	
Ba^{2+}	$5s5p^5 5d^2$	90	221 033.2–221 019.0	50.1–64.3	25.6–48.1
Ba^{3+}	$5p^4 5d$	28	221 031.2–221 019.8	52.1–63.5	27.6–47.3
Ba^{3+}	$5s5p^6$	1	22 028.7	54.6	
Ba^{3+}	$5s5p^5 5d$	23	221 013.7–221 001.2	69.6.82.1	45.1–65.9
Ba^{4+}	$5p^4$	5	221 002.7–220 995.8	80.6–87.5	
Ba^{+}	$4d^9 5s^2 5p^6 5d^2$	67	221 000.8–220 994.9	82.5–88.4	58.0–72.2
Ba^{+}	$4d^9 5s^2 5p^6 4f^2$	107	220 995.0–220 973.8	88.3–109.5	63.8–93.3
Ba^{2+}	$4d^9 5s^2 5p^6 4f$	20	220 992.6–220 965.3	90.7–118.0	
Ba^{2+}	$4d^9 5s^2 5p^6 5d$	18	220 990.8–220 984.7	92.5–98.6	68.0–82.4
Ba^{3+}	$4d^9 5s^2 5p^6$	2	220 972.0–220 969.4	111.3–113.9	
Ba^{5+}	$5p^3$	5	220 945.0–220 938.2	138.3–145.1	
Ba^{4+}	$4d^9 5s^2 5p^5$	12	220 924.1–220 917.9	159.2–165.4	
Ba^{+}	$4p^5 4d^{10} 5s^2 5p^6 5d^2$	45	221 000.8–220 994.9	182.4–201.1	157.9–184.9
Ba^{2+}	$4p^5 4d^{10} 5s^2 5p^6 4f$	12	220 891.9–220 871.9	191.4–211.4	
Ba^{2+}	$4p^5 4d^{10} 5s^2 5p^6 5d$	12	220 890.7–220 874.5	192.6–208.8	168.1–192.6
Ba^{3+}	$4p^5 4d^{10} 5s^2 5p^6$	2	220 872.0–220 856.5	211.3–226.8	

tions the relativistic Dirac-Fock computer code of Grant, McKenzie, and Norrington[45] was employed. Direct-ionization cross sections for the $5p$, $5s$, and $4d$ subshells were computed using a nonrelativistic distorted-wave code.[46] Ground-state correlation was included in some of the cross-section calculations as noted in the text. No attempts were made to calculate excitation-autoionization and resonance contributions to net single or double ionization.

Figure 1 presents an energy-level diagram for relevant configurations of Ba^{q+} ions ($q=1,2,\ldots,5$). Numerical values are given in Table I.

IV. DISCUSSION OF RESULTS

The first few ionization stages of barium are among the most interesting heavy ions in the Periodic Table. Between neutral barium and Ba^{3+} major changes occur in two important dipole-allowed excitation channels, $5p^6 \rightarrow 5p^5 kd$ and $4d^{10}5s^25p^n \rightarrow 4d^95s^25p^n kf$, where k represents a bound or continuum state. The potentials from which these excited orbitals are derived have a double-well character, with the $1s-5p$ core orbitals closely overlapping the innermost well. For the neutral and the first ion, the kd and kf states reside in the outer potential well. They have only a small overlap with the core orbitals and thus have a very diffuse distribution of excitation oscillator strength. Between the first and the third ionization state, however, a major change occurs in these channels wherein the excited orbitals collapse into the inner well where the overlap with the core orbitals is much greater. This collapse of the excited orbitals has a profound effect on the oscillator-strength distribution. For low-ionization stages, where the excited orbitals reside in the outer well, there is little oscillator strength in the bound states. Because of the requirement to conserve the total oscillator strength, a small bound-bound component necessitates a large continuum contribution. After the collapse, however, the situation is reversed, and the bound states acquire a large fraction of the available oscillator strength, reducing the contribution from the continuum. Ba^{2+} is particularly interesting in that it straddles the collapse of the $4d^9kf$ channel. It has strong bound-bound and bound-continuum features. Lucatorto *et al.*[47] studied the redistribution in $4d$ oscillator strength in photoabsorption experiments. Clark[48] has described the effect in terms of term dependence in the Hartree-Fock Hamiltonian.

In addition to the radical redistribution of the $4d$ excitation oscillator strength, there is also the possibility for shape resonances in the scattering channels for these ions. Shape resonances correspond to the temporary localization of a continuum electron in an inner well of a multiwell potential.

This localization causes abrupt changes in the cross sections associated with any processes involving those partial waves. Hence one can expect a rich variety of cross-section features in electron-impact single and multiple ionization of barium ions. Such features can be especially well studied by the energy-scanning technique (mode 2).

A. Single ionization of Ba^{2+} ions

Figure 2 shows a comparison of cross-section data for single ionization of Ba^{2+} taken with the two different ion sources together with theoretical results for ground-state and metastable parent ions. The PIG data have an onset that agrees with the theoretical threshold of 34.9 eV for single ionization of ground-state Ba^{2+} ions (configuration $5s^25p^6$). The onset of the ECR cross section occurs at 17 eV which suggests a larger population in the $5s^25p^55d$ or possibly $5s^25p^54f$ metastable levels.

Figure 3(a) displays the total single ionization cross section $\sigma_{2,3}$ for Ba^{2+} ions produced in the ECR ion source. The electron energy covers a range from about 10 to 1000 eV. There are distinct steps in the cross section at around 35 and 80 eV measured using the mode-1 technique. In the limited-energy range from 10 to 200 eV scan measurements applying mode 2 were performed. The result is displayed in Fig. 3(b) after normalization to the absolute cross sections from Fig. 3(a). Already on this scale distinct resonance features in the vicinity of 90 eV become visible. The next blowup [Fig. 3(c)] shows the scan data in the energy range from 80 to 100 eV. A number of narrow peaks are found with amplitudes around 3% relative to the total cross section.

One more blowup (using ions from a Penning ion source) is shown in Fig. 3(d) with an energy range from 89.0 to 90.2 eV. In this range a single peak in the cross section is found. After a somewhat arbitrary subtraction of a smooth background, the isolated peak can be displayed. It can be represented by a Gaussian distribu-

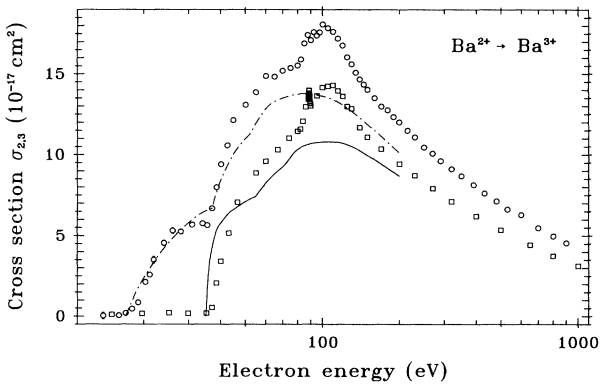

FIG. 2. Absolute cross sections for single ionization of Ba^{2+} ions. Open squares represent measurements employing a "cold" Penning ion source (low content of metastable ions in the parent beam); the open circles are measurements employing a "hot" ECR ion source (producing a substantial amount of metastable ions in the parent beam). The statistical uncertainties are smaller than the size of the symbols. The solid line is a distorted-wave calculation for direct ionization of the $5p$ and $5s$ subshells of ions in the $5s^25p^6$ ground-state configuration. The chain curve is a distorted-wave calculation for direct ionization of the $5p$ and $5s$ subshells of ions in the $5s^25p^55d$ metastable configuration.

tion with 0.39 eV FWHM. This width is an upper limit to the energy spread in the present experiment.

More details of the cross section $\sigma_{2,3}$ for single ionization of Ba^{2+} ions in the energy ranges 30–50 eV and 165–205 eV are displayed in Fig. 4. The results for ground-state and metastable Ba^{2+} parent ions are discussed separately as follows.

1. *Ground-state Ba^{2+} ions, single ionization*

The distorted-wave calculation for ionization of the $5p$ subshell in the ground-state ion models the very rapid rise in the single ionization (PIG) cross section, a feature associated with the double-well nature of the potential for the kd states in barium. Excitation-autoionization involving $5s$ electrons (e.g., $5s^2 5p^6 \rightarrow 5s 5p^6 nl \rightarrow 5s^2 5p^5 + e$) can also contribute to the cross section immediately above the single ionization threshold [see also the data in Fig. 4(a)]. At about 42 eV there is a knee in the curve where the slope of the cross section decreases. This is less pronounced in the experimental data than in the calculation, but could be masked by the onset of $5s$ subshell ionization at 54.6 eV. The most significant difference between the distorted-wave calculations for direct ionization and the observed cross section is the broad feature between 80 and about 120 eV. Energy-scan data (Fig. 5) taken with the mode-2 technique show this maximum to be composed of a large number of individual resonances,

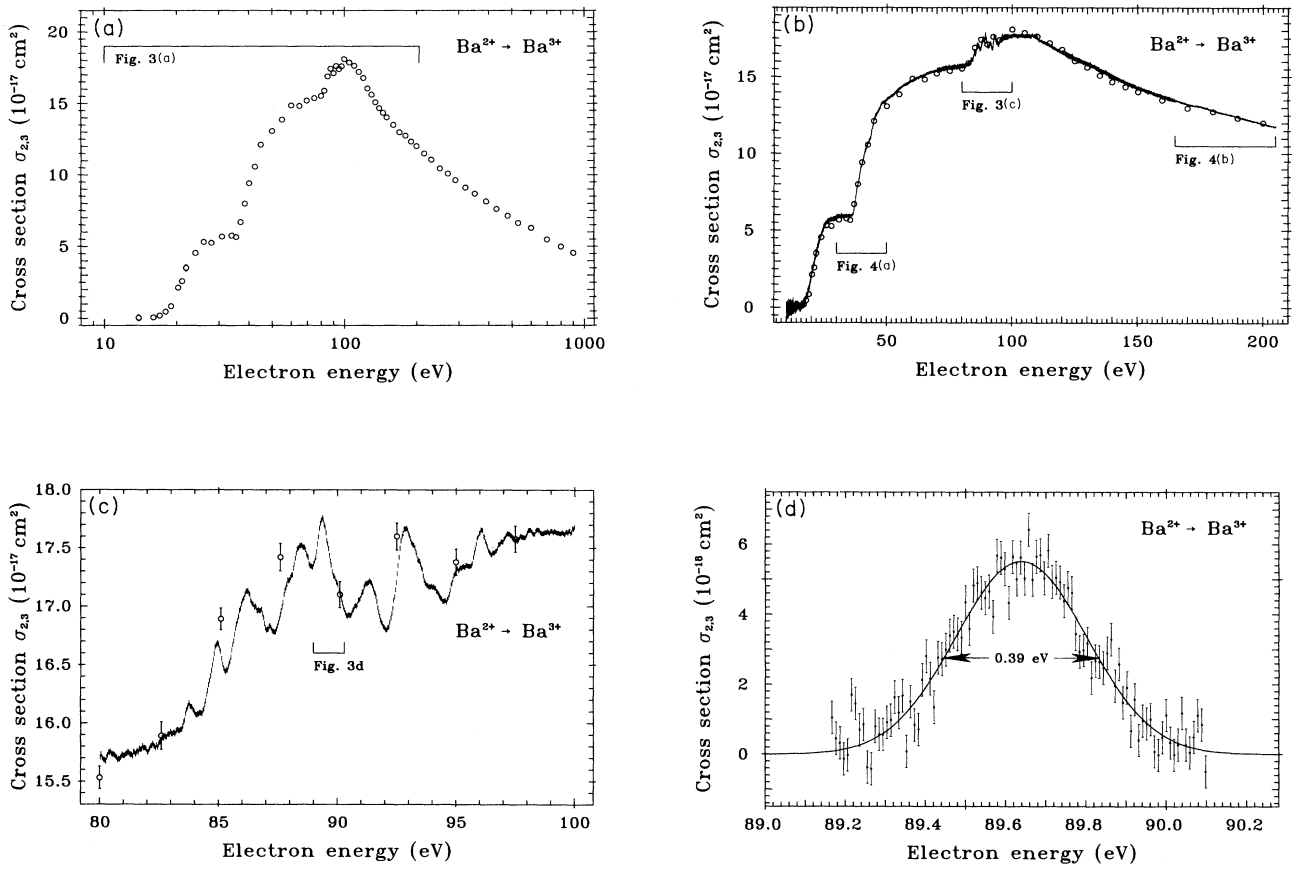

FIG. 3. (a)–(c) Measured electron-impact ionization cross sections for single ionization of Ba^{2+} ions produced with an ECR ion source and (d) a Penning ion source, respectively. (b)–(d) Blowups of particular energy regions. The data were taken by employing the two techniques (modes 1 and 2) described in Sec. II. Horizontal brackets indicate energy intervals for which enlarged plots are also displayed; the numbers and letters identify the respective figures. Open circles represent the absolute cross-section data taken with mode-1 technique. The scan data (mode 2) are normalized to these absolute data. They are displayed as vertical bars indicating the statistical uncertainty. The statistical uncertainties of absolute cross-section measurements are shown where they exceed the size of the symbols. (c) The data were smoothed by using the running average over five measured points. (d) Obtained by performing a scan measurement with ions from a Penning ion source and an increased density of points (10 meV spacing). A smooth "background" curve was subtracted from the measured cross sections in order to better visualize one single peak in the cross section displayed in (d). (d) The solid curve is a fit of the experimental data with a Gaussian distribution. The FWHM is 0.39 eV.

with widths of less than 1 eV.

Energy-level calculations demonstrate that many of these features must be associated with recombination followed by double autoionization (REDA). A likely transitions array is $4d^{10}5s^25p^6+e\rightarrow 4d^95s^25p^65d^2$ which contains 67 resonances between 82.5 and 88.4 eV. Resonances involving a $4d\rightarrow 4f$ excitation such as

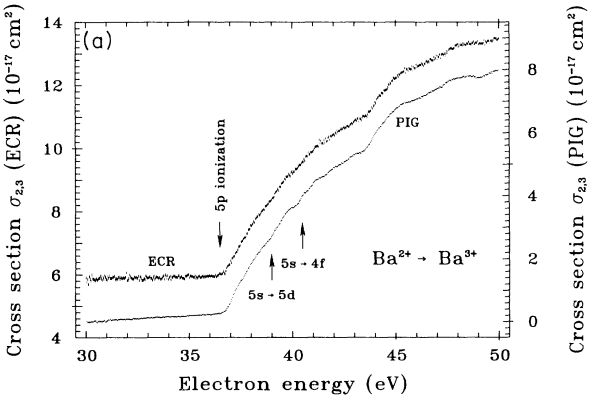

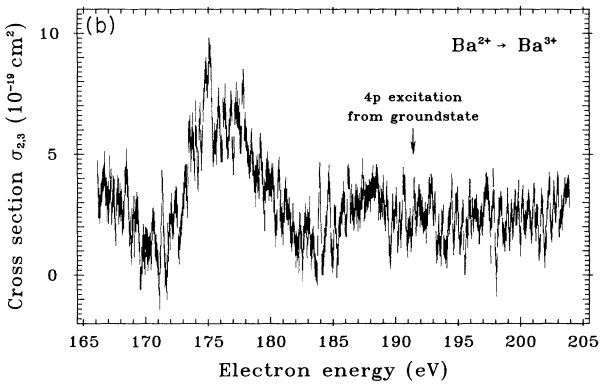

FIG. 4. Details of the Ba^{2+} single ionization energy scan displayed in Fig. 3(b) and (a) comparison of data taken with different ion sources. (a) Below 36.5 eV a contribution is seen from $5p^55d$ and $5p^54f$ metastable states in the parent ECR ion beam which is very weak in the measurements with ions from the Penning ion source. Structure in the cross section above 36.5 eV is probably due to resonant and nonresonant excitation of the $5s$ subshell in ground-state and metastable Ba^{2+}; arrows indicating $5s\rightarrow 5d$ and $5s\rightarrow 4f$ excitations point to features seen in the experiment cross sections. (b) The energy range displayed contains contributions from $4p$ subshell excitations (of ions from the ECR ion source only). The threshold for direct (nonresonant) excitation of a $4p$ electron in ground-state Ba^{2+} is indicated. The resonances observed below this threshold may arise both from ground-state and metastable Ba^{2+} parent ions. The experimental scan data were smoothed using a running average over five points. A straight line representing the nonresonant "background" is subtracted. The arrow indicates the lowest theoretical threshold of $4p$ excitations from ground-state Ba^{2+}.

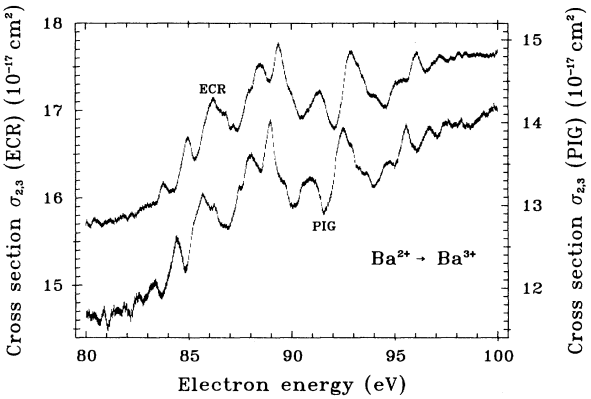

FIG. 5. Comparison of energy-scan data for single ionization of Ba^{2+} ions produced with an electron-cyclotron-resonance ion source (ECR) and a Penning ion source (PIG). Both data sets were smoothed by using the running average over five points. No correction for energy shift by changing contact potentials was made.

$4d^{10}5s^25p^6+e\rightarrow 4d^95s^25p^64f^2$ can also contribute. There are 107 separate resonances in this array in the energy range 88.3–109.5 eV. The $5d4f$ combination is also possible as are more complex configurations $4d^95s^25p^6nln'l'$ which occur at higher energies. The series limit of these resonances is 111.3 eV, the ionization threshold for a $4d$ electron. As Clark and others have pointed out, the distribution of optical oscillator strength in Ba^{2+} among the $4d-nf$ transitions is quite complex, owing to the double-well potential determining the nf wave functions and the influence of intermediate coupling.[48] Levels within the $4d^9nf\,^1P$ excited terms are strongly separated by term-dependent electrostatic and spin-orbit interactions. Rather than a monotonic decrease with increasing n, the optical oscillator strength peaks at $n=5$. If this trend follows over into recombination excitation processes, one would expect a similar wide distribution of the resonances. Note that the intermediate state associated with recombination excitation $4d^95s^25p^6nln'l'$ can decay via two sequential single autoionization processes, i.e., $4d^95s^25p^6nln'l'\rightarrow 4d^{10}5s5p^6nl+e\rightarrow 4d^{10}5s^25p^5+2e$.

Excitation-autoionization processes involving $4d$ electrons can also occur. The thresholds for $4d^{10}5s^25p^6\rightarrow 4d^95s^25p^64f$ excitations are in the range 90.7–118.0 eV, the higher energies corresponding to the diffuse ^1P orbital. Similar excitations involving a $5d$ excited electron occur in the range 92.5–98.6 eV. Excitation-autionization features can thus contribute to the broad feature in the observed cross section only above 90 eV, leaving the span 80–90 eV the sole domain of resonant-excitation processes. Dielectronic capture resonances involving $4p$ electrons can result in net single ionization of the target at energies above 180 eV. There is some indication of such resonances in the ECR data [see Fig. (4b)].

2. *Metastable Ba^{2+} ions, single ionization*

Distorted-wave calculations for direct single ionization of Ba^{2+} assuming 100% population of $5p^5 5d$ metastable levels are in good agreement with the ECR data up to about 30 eV. This agreement may be fortuitous, however, owing to the presence of excitation-autoionization processes such as $5p^5 5d \rightarrow 5p^4 5d^2 \rightarrow 5p^5 + e$ which occur close to threshold. The thresholds for ionization of a $5p$ electron in the $5p^5 5d$ metastable configuration are in the range 27.6–47.3 eV, so that direct ionization of the $5p$ subshell will contribute above these energies. From 50–80 eV the observed cross section is somewhat larger than the theoretical cross section for direct ionization. This may be due to a combination of the inaccuracy of the direct-ionization cross-section calculation and the presence of excitation-autoionization features of the type $5s^2 5p^5 5d \rightarrow 5s 5p^5 5d^2$, which have thresholds in the range 25–47 eV [see Fig. 4(a)]. Mixing of a ground-state population in the beam will further increase the $5p$ contribution above the $5p^6 \rightarrow 5p^5$ direct-ionization threshold. It is not possible to determine the metastable content of the beam by a comparison of theory to experiment owing to the uncertainty of the theoretical cross sections and the overlap of the thresholds for various processes.

The structure in the cross section around 80 eV is most likely due to recombination resonances of a type similar to those discussed for the Penning source data. Excitation autoionization from the $4d$ subshell will also contribute to the cross section. These features are potentially more complex for an ion in a metastable initial state owing to the larger number of couplings allowed for the $5p^5 5d$ configuration versus a $5p^6$ closed initial configuration.

As mentioned above, the ECR scan data in the energy range 170–200 eV are consistent with the presence of dielectronic capture involving $4p$ subshell electrons and subsequent double autoionization [see Fig. (4b)].

It is interesting to note that the resonance features found in the energy range 80–100 eV with ECR and PIG Ba^{2+} ions are nearly identical. This is shown in Fig. 5, where normalized energy scans taken with ions from the ECR and Penning ion sources are compared.

Since we suspected a near 100% metastable $5p^5 5d$ or $5p^5 5f$ population of the ECR ion beam, a much more complex spectrum of resonances due to the increased number of couplings would have been plausible. Apparently, however, the resonances involving $4d \rightarrow nl$ excitations are not influenced much by the electron configuration of the outermost subshells.

B. Double ionization of Ba^{2+} ions

A set of data similar to those discussed above has been taken for double ionization of Ba^{2+} ions. Absolute cross sections $\sigma_{2,4}$ for Ba^{2+} ions from the ECR and the Penning ion sources are displayed in Fig. 6 together with distorted-wave calculations. Again the PIG data are below the ECR data. No significant difference in the double ionization onset is seen although the single ionization data suggested a near 100% metastable population in the ECR ion beam. For double ionization of $5p^5 5d$ and $5p^5 4f$ metastable Ba^{2+}, one would expect an onset in the energy range 55–66 eV. The experiment shows that only above the threshold for ionization of two $5p$ electrons is there an appreciable cross section. This suggests an interpretation of double ionization involving a strong correlation between equivalent target electrons. Excitations such as $4d^{10} 5s^2 5p^6 \rightarrow 4d^9 5s^2 5p^6 nl$ can contribute to double ionization above 91 eV through auto-double-ionization of the excited state. A single autoionization leads to a bound state and hence to single ionization of the target. The observed stepwise increase of the cross section above 90 eV [see Fig. 8(a)] is consistent with the presence of excitation followed by auto-double-ionization.

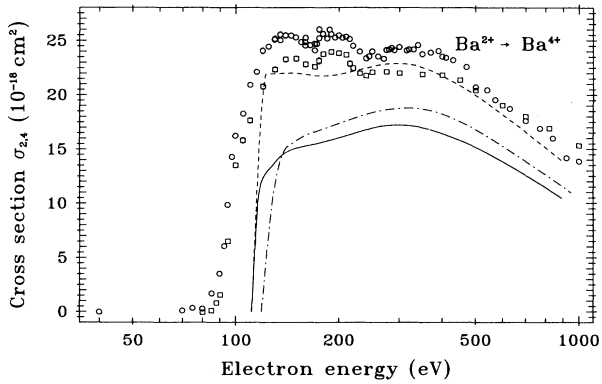

FIG. 6. Absolute cross sections for double ionization of Ba^{2+} ions. Open squares represent measurements employing a "cold" Penning ion source (low content of metastable ions in the parent beam); the open circles are measurements employing a "hot" ECR ion source (metastable ions in the parent beam). The statistical uncertainties are smaller than the size of the symbols. The theoretical curves represent distorted-wave calculations for direct ionization of the $4d$ subshell of ions in the $5s^2 5p^6$ ground-state configuration (solid line), in the $5s^2 5p^5 5d$ metastable configuration (chain curve), and in the $5s^2 5p^5 4f$ metastable configuration (dashed line).

Ionization of a $4d$ electron will lead to effective double ionization of Ba^{2+} by autoionization of the residual ion: $4d^{10} 5s^2 5p^6 + e \rightarrow 4d^9 5s^2 5p^6 + 2e \rightarrow 4d^{10} 5s 5p^5 + 3e$. The theoretical threshold for $4d$ direct ionization is 111 eV. The first maximum in the cross section, occurring at about 130 eV corresponds to the expected location of a shape resonance in the $4d$ direct-ionization cross section. This resonance is present in distorted-wave calculations of the $5p^5 4f$ configuration. A weaker effect was calculated for the ground configuration. It was noted in the calculations, however, that the cross section was very sensitive to the details of the potentials used to compute the partial waves. This is because the kf channels in Ba^{2+} are on the verge of collapse from the diffuse outer potential well to the compact inner well which closely overlies the $4d$ subshell. Thus the actual shape resonance may be more pronounced than our calculations indicate.

The broad feature between 170 and 220 eV may be associated with several different kinds of resonant fea-

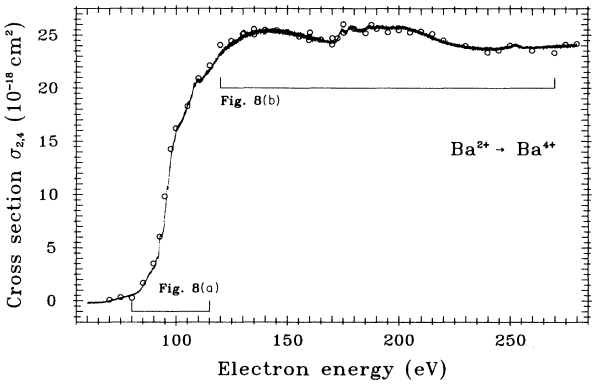

FIG. 7. Energy-scan cross sections for double ionization of Ba^{2+} ions produced by an ECR ion source. The scan data were normalized to the absolute measurements represented by open circles. The horizontal brackets indicate energy intervals for which enlarged plots are displayed in Fig. 8.

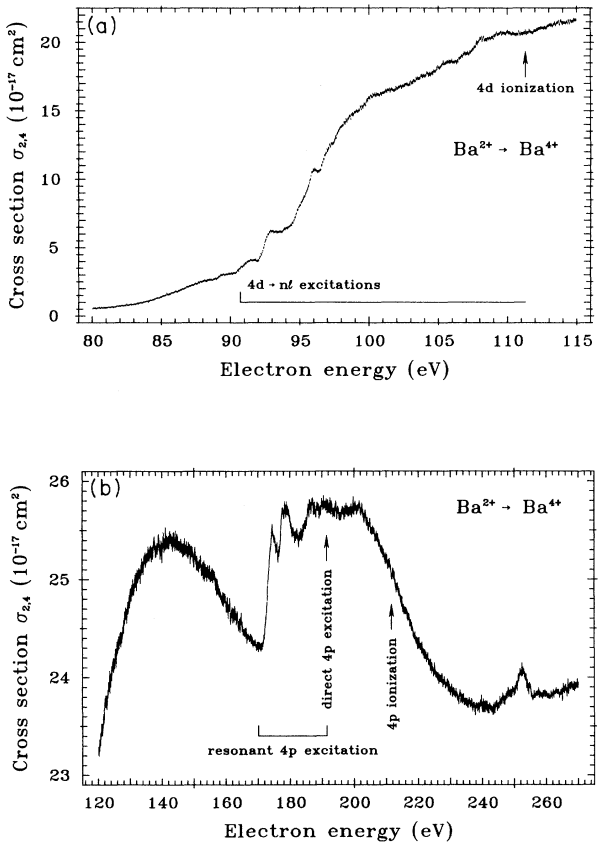

FIG. 8. Energy-scan cross sections for double ionization of Ba^{2+} ions produced by an ECR ion source (details from Fig. 7). Energies for 4*d*- and 4*p*-vacancy production are indicated. (a) Energy range 80–115 eV; (b) energy range 120–270 eV (smoothed over five original data points).

tures. Between 180–200 eV one expects a series of recombination resonances (e.g., $4p^6 4d^{10} 5s^2 5p^6 + e \rightarrow 4p^5 4d^{10} 5s^2 5p^6 5d^2$) involving 4*p* excitations followed by two sequential autoionizations, one of which involves a double-electron emission. Excitation of a 4*p* electron followed by two sequential single autoionziation events is possible above 191 eV. The ECR data displayed in Figs. 7 and 8(b) show clear evidence of such resonances between 170 and 200 eV. (The lower thresholds of the observed resonances are consistent with a metastable content in the ECR beam.) Direct ionization of the 4*p* subshell will most likely result in triple ionization of a ground-state ion, since the 4*p* hole will be filled by an Auger transition from the 4*d* subshell, which will leave an autoionizing 4*d* hole configuration. The broad feature above 200 eV may be the normal maximum of the 4*d* subshell ionization cross section.

The contributions of many resonant processes along with direct double ionization results in poor agreement between the computed cross section for direct ionization of the 4*d* subshell and the observations.

C. Comparisons of features in $\sigma_{2,3}$ and $\sigma_{2,4}$

The energy-scan measurements displayed in Fig. 8(a) reveal a wealth of structure in the double ionization cross section just above threshold. Many of the features look like excitation (multiple) -autoionization events. Our interpretation, however, is that we see resonance peaks sitting on the steep slope of a rapidly rising cross section for direct double ionization. This hypothesis is supported by the following considerations. The narrow peaks found in single ionization of Ba^{2+} between 80 and 100 eV (Fig. 5) leave no doubt that we see resonant excitation with subsequent emission of two electrons. These resonances are associated with multiply excited states in Ba^+ with a 4*d* vacancy. There are a number of possibilities for their decay via photoemission and/or electron ejection. Apparently, there is a substantial probability for the emission of two electrons as evidenced by the peaks in $\sigma_{2,3}$. For a sufficiently high degree of excitation of the intermediate compound state of the electron and the parent ion, one can also expect a certain probability for the emission of more than two electrons which would result in resonance features in multiple ionization cross sections. These resonances occur at the same energies as in single ionization since they are related to the same intermediate resonant states in the compound Ba^+ ion. Hence, if the structures found in the cross section $\sigma_{2,4}$ for double ionization of Ba^{2+} are due to dielectronic (resonant) capture and subsequent emission of three electrons, then these resonances have to line up in energy with the peaks observed in $\sigma_{2,3}$. By comparing energy positions of features in Figs. 3(c) and 8(a) one finds this condition fulfilled (see Fig. 9). A different way of displaying the data makes the relation between features in $\sigma_{2,3}$ and $\sigma_{2,4}$ obvious. By subtracting smooth "background" curves (as indicated in Fig. 9) from the measured cross sections one can emphasize the observed structures. Background in this context includes direct-ionization processes with no sharp features in the cross section. Results of such sub-

tractions are displayed in Fig. 10 for $\sigma_{2,3}$ and $\sigma_{2,4}$. The original cross sections were measured with ions from the ECR ion source. The resonance features in $\sigma_{2,3}$ and $\sigma_{2,4}$ line up perfectly thus lending convincing support to the hypothesis discussed above. Multiply excited states in an intermediate Ba^+ compound ion decay in these examples via emission of two and three electrons. The probability for the emission of three electrons appears to be roughly a factor of 5 smaller than that for two-electron emission. Of course, there is some arbitrariness in the subtraction of a smooth curve so that peak heights appear different when different "backgrounds" are subtracted. Towards the lower energies the resonances in $\sigma_{2,4}$ appear to die out. In particular the peak in $\sigma_{2,4}$ related to the dominant resonance in $\sigma_{2,3}$ at 89.6 eV is hardly visible. This behavior becomes plausible when one considers the threshold for double ionization of Ba^{2+}. States in the $5s^25p^4$ configuration are 80.6–87.5 eV above the $5s^25p^6$ ground-state configuration. In the vicinity of the threshold region the available phase space for the emission of three electrons from the intermediate resonant states in Ba^+ certainly becomes more and more limited and hence the related decay probabilities decrease. As a result the peak heights in the double ionization cross section go down when the threshold is approached.

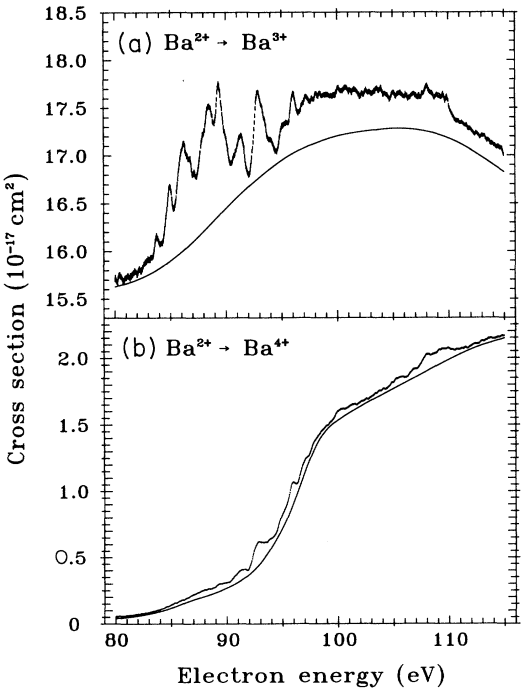

FIG. 9. Comparison of cross sections for (a) single and (b) double ionization of Ba^{2+} ions (produced in an ECR ion source). Both data sets were smoothed over five original data points. Due to the gross energy dependence of the cross sections, it is difficult to see corresponding fine details in the scan data. Therefore, smooth curves representing nonresonant background are subtracted (see Fig. 10). The solid lines in this figure are used for the subtraction.

D. Single ionization of Ba^{3+} ions

The cross sections discussed so far were for Xe-like Ba^{2+} ions. Comparable measurements and calculations were carried out also for I-like Ba^{3+} ions. We show in Fig. 11 absolute cross-section measurements for single ionization of Ba^{3+} together with distorted-wave calculations for direct single ionization of the $5p$ and $5s$ subshells. Again there are two sets of data obtained with ions from the ECR and Penning ion sources, i.e., with beams containing different fractions of metastable ions.

1. Ba^{3+} ground-state ions, single ionization

The solid squares in Fig. 11 are the data obtained with the Penning ion source, which is assumed to deliver mainly ground-state Ba^{3+} ions. This assumption is justified by the onset of the cross section near 45 eV, which is close to the predicted threshold for ionization of a $5p$ electron of a ground-state Ba^{3+} ion.

Excitation-autoionization resonances involving $5s$ electrons occur just above the $5p^4$ threshold and hence can

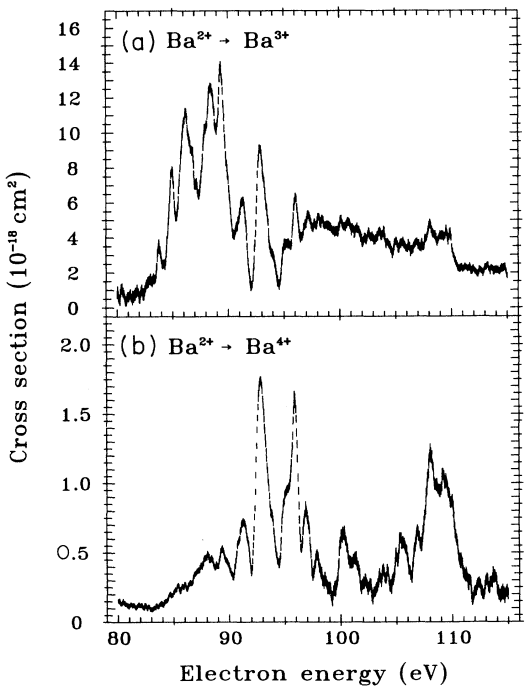

FIG. 10. Subtracted cross sections (a) $\sigma_{2,3}$ for single and (b) $\sigma_{2,4}$ for double ionization of Ba^{2+}. From the measured scan data the smooth curve displayed in Fig. 9 were subtracted in order to visualize the cross-section features. Strucutres and peaks in $\sigma_{2,3}$ and $\sigma_{2,4}$ line up in energy.

contribute to single ionization. Some of the lowest such configurations, like $5s5p^5 5d$, are split across the ionization threshold, so that only some of the levels will contribute to ionization. A significant difference in the ionization of Ba^{2+} and Ba^{3+} is the availability of a vacancy in the $5p$ subshell of the latter ion which can accept excitations from the $4d$ subshell. This provides additional paths for excitation plus autoionization and also for resonant excitation (involving dielectronic capture) followed by a double auotionization process. The thresholds for $4d \rightarrow 5p$ resonant excitations $4d^{10}5s^2 5p^5 + e \rightarrow 4d^9 5s^2 5p^6 5d$ are in the range 55.4–63.7 eV, compared to the approximately 80 eV required to promote a $4d$ electron to a $5d$ state. If these resonances contribute to single ionization, they must do so by a two-electron autoionization, since a single-electron emission leads to a bound state with no net ionization of the target. Excitation of a $4d$ electron to the $5p$ hole $4d^{10}5s^2 5p^5 \rightarrow 4d^9 5s^2 5p^6$ occurs above the threshold range 74.2–79.0 eV, and thus leads to net ionization via a single autoionization.

The shape of the $Ba^{3+} \rightarrow Ba^4$ cross section is generally similar to that of $Ba^{2+} \rightarrow Ba^{3+}$, with clear indications of sharp resonances at approximately 80 eV (see Fig. 12), and a pronounced peak centered around 100 eV. With the exception of the $4d \rightarrow 5p$ excitations (resonant, i.e., via dielectronic capture, and nonresonant, i.e., via direct excitation) which may contribute in the range above 55 eV, the mechanisms for ionization of Ba^{3+} are expected to be analogs of those already discussed for Ba^{2+}. Thus below 55 eV direct ionization and $5s$ excitation-autoionization contribute to the cross section. Above 55 eV resonant-excitation double autoionization involving $4d \rightarrow 5p$ excitations occurs. Excitation autoionization involving $4d \rightarrow 5p$ transitions takes place above 74 eV. Around 80 eV $4d \rightarrow (5d, 4f)$ resonant excitations can lead to the same type of sharp resonances as those found in Ba^{2+}. In contrast to Ba^{2+}, however, the lowest dielectronic capture resonances in Ba^{3+} must decay via a two-electron emission, since a single autoionization event will result in a bound state with no net ionization of the target ion. For example, the dielectronic capture $4d^{10}5s^2 5p^5 + e \rightarrow 4d^9 5s^2 5p^5 5d^2$ is followed by an autoionization to $4d^{10}5s5p^5 5d + e$, most of the levels of which are below the threshold for further autoionization. Higher Rydberg levels excited by dielectronic capture can contribute to the single ionization cross section via two sequential autoionizations. It is interesting that the sharp resonances observed in Ba^{3+} (see Fig. 12) occur at lower incident electron energies than in Ba^{2+} [see e.g., Fig. 3(b)]. This is consistent with excitations to nf levels which are undergoing rapid radial contraction with increasing ionization of the target. In Ba^+ the $4f$ orbital associated with the $4d^9 4f\,^1P$ excitation resides in the outer well of a double-well potential. In Ba^{2+} the orbital is partially contracted and in Ba^{3+} has collapsed to smaller radii comparable to the mean radius of the $4d$ subshell.

Agreement between experiment and distorted-wave theory for the direct ionization is poor, owing to the presence of $5s$ excitation autoionization just above threshold and the strong $4d$ excitations about 74 eV.

The larger feature in the $Ba^{3+} \rightarrow Ba^{4+}$ cross section

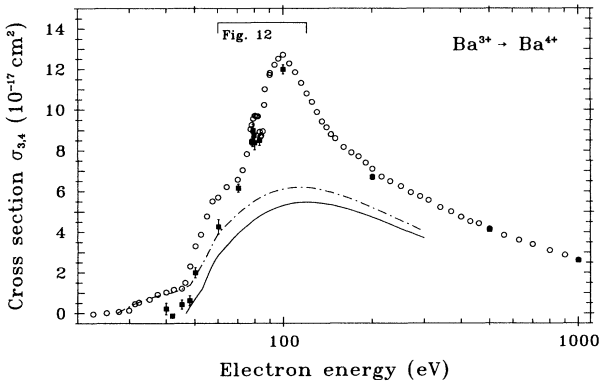

FIG. 11. Absolute cross sections for single ionization of Ba^{3+} ions. Data were taken with ions produced in an ECR ion source (open circles) and in a Penning ion source (solid squares). Statistical uncertainties are indicated where they exceed the size of the symbols. The theoretical curves represent distorted-wave calculations for direct ionization of the $5p$ and $5s$ subshells of parent ions in the $5s^2 5p^5$ ground-state configuration (solid line) and of the $5d$, $5p$, and $5s$ subshells of parent ions in the $5s^2 5p^4 5d$ metastable configuration. The chain curve is for an assumed ratio of 40%/60% of metastable and ground-state ion content in the parent beam. This ratio was chosen to give optimum agreement with the experiment data below the $5p$ ionization threshold. The horizontal bracket indicates the energy range of the scan measurement displayed in Fig. 12.

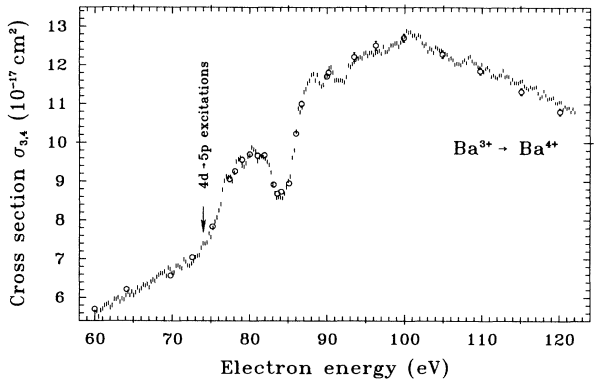

FIG. 12. Energy-scan cross sections for single ionization of Ba^{3+} ions produced by an ECR ion source (details from Fig. 11). The scan data are normalized to absolute measurements (solid circles). Excitations of the $4d$ subshell are possible at energies up to 125 eV, the ionization threshold for $4d$ electrons. The arrow indicating $4d \rightarrow 5p$ excitations points to the experimental change in slope at 74 eV.

peaking at 100 eV is most likely due to excitations from the $4d$ subshell followed by autoionization.

2. Ba^{3+} metastable ions, single ionization

The experimental data obtained with the ECR source (open circles in Fig. 11) are very similar to those from the Penning source (solid squares in Fig. 11). The principal difference is the presence of metastable component in the beam as evidenced by the ECR cross section rising at approximately 20 eV, well below the threshold for ground-state ionization. The most probable metastable configurations are $5p^4 5d$ and $5p^4 4f$. The excited electron in the metastable configuration will also permit excitation-autoionization resonances of the type $5s^2 5p^4 5d \rightarrow 5s 5p^4 5d^2$ to contribute to the cross section. The chain curve in Fig. 11 is a distorted-wave calculation for direct ionization of the $5p$ and $5s$ subshells of Ba^{3+} ions in a beam containing 60% ground-state ions ($4d^{10} 5s^2 5p^5$) and 40% metastable ions ($4d^{10} 5s^2 5p^4 5d$). The metastable content was adjusted to fit the experimental data below the ground-state ionization threshold near 45 eV. There is no other justification for assuming that mixture ratio.

E. Double ionization of Ba^{3+} ions

The intensity of the Ba^{3+} ion beam from the Penning ion source was not sufficient for an accurate double ionization cross-section measurement. Hence, only data obtained with the ECR ion source are available. These are shown in Fig. 13.

The threshold for direct double ionization of the $5p^5$ ground-state is 101 eV. That the observed cross section begins to rise at 90 eV is consistent with the interpretation of a small $5p^4$ $(5d,4f)$ metastable component to the beam. This is interesting since for $Ba^{2+} \rightarrow Ba^{4+}$, where the ECR beam apparently contained a much larger metastable fraction, the cross section did not rise until after the threshold for ionization of two equivalent $5p$ electrons. Excitation of a $5s$ electron, which could be followed by an auto-double-ionization cannot be the explanation, since it occurs at too low an energy. Conversely, ionization of a $4d$ electron occurs at too high an energy. Excitation of a $4d$ electron to an autoionizing configuration could occur in this energy range, particularly to the $5p$ hole, but the resulting excitation would have to decay via auto-double-ionization to result in net double ionization of the target. Thus the most probable explanation of the low-energy rise in the cross section is the direct double ionization of a $5p+(5d,4f)$ electron pair, the thresholds for which are in the range 74–90 eV. An explanation for the participation of the excited orbital in direct double ionization may be the greater degree of collapse of the kd and kf channels in Ba^{3+} compared to Ba^{2+}, leading to stronger correlations between the excited and core orbitals.

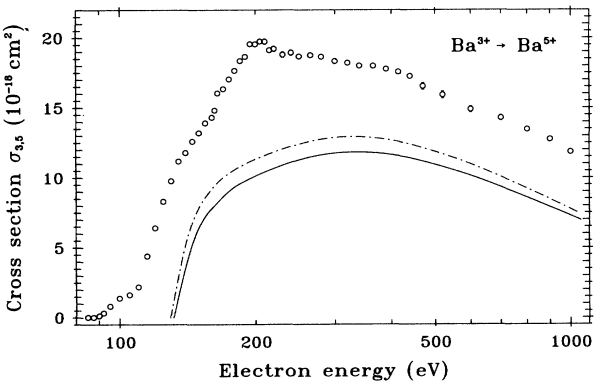

FIG. 13. Absolute cross sections for double ionization of Ba^{3+} ions. The data were taken with ions produced in an ECR ion source. Statistical uncertainties are smaller than the size of the symbols. The theoretical curves are distorted-wave calculations for direct ionization of the $4d$ subshell of ions in the $5s^2 5p^5$ ground-state configuration (solid line) and the $5s^2 5p^4 5d$ metastable configuration (chain curve).

The rapid rise in the cross section near 110 eV corresponds to the threshold for ionization of a $(5p,5p)$ electron pair. The thresholds for ionization processes $5p^5 + e \rightarrow 5p^3 + 3e$ and $5p^4 5d + e \rightarrow 5p^3 + 3e$ are almost identical. Ionization of a $4d$ electron, followed by single autoionization of the residual ion, occurs above 122 eV.

The pronounced bump in the cross section centered at 200 eV is probably due to $4p$ excitations. It is well above the $4d$ ionization limit and hence cannot be associated with any excitation from that subshell. Ionization of the $4p$ subshell does not occur until about 220 eV and leads to net triple ionization via two sequential autoionizations of the $4p$ hole. It is unlikely that it is associated with any deeper subshells, which have characteristically higher energies.

As in the case of double ionization in Ba^{2+}, distorted-wave calculations for $4d$ ionization poorly represent the observed cross section, indicating that direct double ionization (at lower energies) and processes involving resonant and nonresonant excitations (with and without dielectric capture) are important components.

V. CONCLUSION

Cross sections for electron-impact single and double ionization of Ba^{2+} and Ba^{3+} ions have been measured. By using two different ion sources, parent-ion beams with and without metastable contents could be employed. "Without" in this context means that no ionization signal could be detected below the threshold for ionization of ground-state ions. The data thus collected yield information on the influence of metastable states on the ionization cross sections.

The use of a very sensitive energy-scanning technique made it possible for us to detect fine details in the ionization cross sections. In particular, large contributions involving dielectronic capture and subsequent emission of two or more electrons could be detected. Narrow peaks

with widths as low as 0.39 eV were observed.

Most of the cross-section features can be qualitatively understood on the basis of relativistic Dirac-Fock energy-level calculations. Comparison of the measured cross sections with distorted-wave calculations of direct ionization contributions show the relative importance of excitation-autoionization and resonant contributions, particularly in the higher stages of ionization.

ACKNOWLEDGMENTS

This work was supported partly by Deutsche Forschungsgemeinschaft (DFG) and partly under the auspices of the U.S. Department of Energy. The authors thank G. H. Dunn for stimulating discussions and his cooperation in a series of ionization experiments that were directly related to the present work.

*Present address: Gesellschaft für Schwerionenforschung (GSI), Darmstadt, Germany.

[1]M. Goeppert-Mayer, Phys. Rev. **60**, 184 (1941).

[2]D. C. Griffin, K. L. Andrew, and R. D. Cowan, Phys. Rev. **177**, 62 (1969).

[3]D. C. Griffin and M. S. Pindzola, Comments At. Mol. Phys. **13**, 1 (1983).

[4]S. M. Younger, Phys. Rev. A **22**, 2682 (1980).

[5]D. L. Ederer, Phys. Rev. Lett. **13**, 760 (1964).

[6]T. M. Zimkina, V. A. Fomichev, S. A. Gribovskii, and I. I. Zhukova, Fiz. Tverd. Tela (Leningrad) **9**, 1447 (1967) [Sov. Phys. Solid State **9**, 1128 (1967)]; **9**, 1163 (1967).

[7]J. M. Bizau, D. Cubaynes, P. Gerard, and F. J. Wuilleumier, Phys. Rev. A **40**, 3002 (1989).

[8]M. Richter, M. Meyer, M. Pahler, T. Prescher, E. v. Raven, B. Sonntag, and H. E. Wetzel, Phys. Rev. A **39**, 5666 (1989).

[9]*Giant Resonances in Atoms, Molecules and Solids,* edited by J. P. Connerade, J. M. Esteva, and R. C. Karnatac (Plenum, New York, 1987).

[10]C. Achenbach, A. Müller, E. Salzborn, and R. Becker, Phys. Rev. Lett. **50**, 2070 (1983).

[11]A. Müller, C. Achenbach, E. Salzborn, and R. Becker, J. Phys. B **17**, 1427 (1984).

[12]D. R. Hertling, R. K. Feeney, D. W. Hughes, and W. E. Sayle, J. Appl. Phys. **53**, 5427 (1982).

[13]T. Hirayama, S. Kobayashi, A. Matsumoto, S. Ohtani, T. Takayanagi, K. Waikiya, and H. Suzuki, J. Phys. Soc. Jpn. **56**, 851 (1987).

[14]A. Müller, K. Tinschert, G. Hofmann, E. Salzborn, and G. H. Dunn, Phys. Rev. Lett. **61**, 70 (1988).

[15]M. S. Pindzola, D. C. Griffin, and C. Bottcher, J. Phys. B **16**, L35 (1983).

[16]M. S. Pindzola, D. C. Griffin, C. Bottcher, D. H. Crandall, R. A. Phaneuf, and D. C. Gregory, Phys. Rev. A **29**, 1749 (1984).

[17]S. M. Younger, Phys. Rev. Lett. **56**, 2618 (1986).

[18]S. M. Younger, Phys. Rev. A **35**, 2841 (1987).

[19]S. M. Younger, Phys. Rev. A **35**, 4567 (1987).

[20]S. M. Younger, Phys. Rev. A **37**, 4125 (1988).

[21]A. Müller, K. Tinschert, G. Hofmann, E. Salzborn, G. H. Dunn, S. M. Younger, and M. S. Pindzola, Phys. Rev. A **40**, 3584 (1989).

[22]A. Müller, in *The Physics of Electronic and Atomic Collisions (New York, 1989),* Proceedings of the XVIth International Conference on the Physics of Electronic and Atomic Collisions, AIP Conf. Proc. No. 205, edited by A. Dalgarno, R. S. Freund, P. M. Koch, M. S. Lubell, and T. B. Lucatorto (AIP, New York, 1990), p. 418.

[23]B. Peart and K. T. Dolder, J. Phys. B **1**, 872 (1968).

[24]B. Peart, J. G. Stevenson, and K. T. Dolder, J. Phys. B **6**, 146 (1973).

[25]B. Peart, J. R. A. Underwood, and K. Dolder, J. Phys. B **22**, 1679 (1989).

[26]R. K. Feeney, J. W. Hooper, and M. T. Elford, Phys. Rev. A **6**, 1469 (1972).

[27]D. C. Griffin, M. S. Pindzola, and C. Bottcher, J. Phys. B **17**, 3183 (1984).

[28]K. Tinschert, A. Müller, G. Hofmann, K. Huber, R. Becker, D. C. Gregory, and E. Salzborn, J. Phys. B **22**, 531 (1989).

[29]H. Baumann, and K. Bethge, Nucl. Instrum. Methods **122**, 517 (1979).

[30]G. Mank, M. Liehr, and E. Salzborn, in *Proceedings of the 7th Workshop on Electron Cyclotron Resonance (ECR) Ion Sources,* edited by H. Beuscher (Berichte der Kernforschungsanlage Jülich, No. Jül-Conf-57, Jülich), (available from Zentralbibliothek der Kernforschungsanlage Jülich GmbH, Postfach 1913, D-5170 Jülich, Federal Republic of Germany), pp. 203–214.

[31]R. Becker, A. Müller, C. Achenbach, K. Tinschert, and E. Salzborn, Nucl. Instrum. Methods, Phys. Res. Sec. B **9**, 385 (1985).

[32]K. Rinn, A. Müller, H. Eichenauer, and E. Salzborn, Rev. Sci. Instrum. **53**, 829 (1982).

[33]A. Müller, G. Hofman, K. Tinschert, R. Sauer, E. Salzborn, and R. Becker, Nucl. Instrum. Methods, Phys. Res. Sect. B **24/25**, 369 (1987).

[34]G. Hofmann, A. Müller, K. Tinschert, and E. Salzborn, Z. Phys. D **16**, 113 (1990).

[35]A. Müller, K. Huber, R. Becker, and E. Salzborn, J. Phys. B **18**, 3011 (1985); A. Müller, K. Tinschert, C. Achenbach, E. Salzborn, and R. Becker, Nucl. Instrum. Methods, Phys. Res. Sect. B **10/11**, 204 (1985).

[36]A. Müller, G. Hofmann, B. Weissbecker, M. Stenke, K. Tinschert, M. Wagner, and E. Salzborn, Phys. Rev. Lett. **63**, 758 (1989).

[37]K. J. LaGattuta and Y. Hahn, Phys. Rev. A **24**, 2273 (1981).

[38]R. J. W. Henry and A. Z. Msezane, Phys. Rev. A **26**, 2545 (1982).

[39]D. C. Griffin, C. Bottcher, M. S. Pindzola, S. M. Younger, D. C. Gregory, and D. H. Crandall, Phys. Rev. A **29**, 1729 (1984).

[40]P. G. Burke, A. E. Kingston, and A. E. Thompson, J. Phys. B **16**, L385 (1983).

[41]M. S. Pindzola, C. Bottcher, and D. C. Griffin, J. Phys. B **20**, 3535 (1987).

[42]S. Tayal and R. J. W. Henry, Phys. Rev. A **42**, 1831 (1990).

[43]S. Tayal and R. J. W. Henry, Phys. Rev. A **39**, 3890 (1989).

[44]M. H. Chen, K. J. Reed, and D. L. Moores, Phys. Rev. Lett. **64**, 1350 (1990).

[45]I. P. Grant, B. J. McKenzie, and P. H. Norrington, Comput. Phys. Commun. **21**, 207 (1980).

[46]S. M. Younger, in *Electron Impact Ionization,* edited by T. D. Märk and G. H. Dunn (Springer-Verlag, Berlin, 1985), Chap. 1; Phys. Rev. A **34**, 1952 (1986).

[47]T. B. Lucatorto, T. J. McIlrath, J. Sugar, and S. M. Younger, Phys. Rev. Lett. **47**, 1124 (1981).

[48]C. W. Clark, J. Opt. Soc. Am. B **1**, 626 (1984).